Journal of Analytical Atomic Spectrometry

Microscopic X-ray fluorescence analysis and related methods with laboratory and synchrotron radiation sources†

Plenary Lecture

F. Adams*[a], K. Janssens[a] and A. Snigirev[b]

[a]Department of Chemistry, University of Antwerpen (UIA), B-2610 Wilrijk, Belgium
[b]European Synchrotron Radiation Facility, F-38043 Grenoble, France

The present status of microprobe versions of XRF analysis with tube excitation and with synchrotron radiation sources is reviewed with respect to analytical parameters such as lateral resolution and imaging capability, and achievable detection limits, precision and accuracy. The main characteristics of the method are contrasted with those of other microanalytical techniques. For laboratory source μ-XRF, results with a rotating anode tube equipped with capillary X-ray optics are discussed in terms of sensitivity and achievable lateral resolution. The possibilities of the new third generation synchrotron radiation storage rings, especially those of the European Synchrotron Radiation Facility (ESRF) and its X-ray micro-fluorescence, imaging and diffraction beamline (ID 22) are discussed and related to second generation storage rings. Some characteristic applications are given to illustrate the recent possibilities of the methodologies, in particular for the characterization of atmospheric particles, and in an analytical problem related to archaeology.

Keywords: *Microprobe; X-ray fluorescence; synchrotron radiation; air particulates; archaeological analysis*

A group of instrumental methods of analysis which have increasingly gained in importance in the last decade is that of the sensitive microanalytical methods. These methods provide information on the lateral (two dimensional) and/or in-depth (three-dimensional) distribution of low concentrations of elemental or molecular species within or at the surface of solid samples. Most of them are based on the use of microscopic beams of charged particles or photons to excite the sample locally. An overview of some of these beam type analytical techniques is given in Table 1.

One of the various possibilities for microscopic analysis resides with the use of X-rays. One century after the discovery of X-rays, XRF analysis[1–3] has developed into a well-established and mature multi-element analytical technique for macroscopic samples. Inner shell ionization in conjunction with X-ray emission relying on excitation with electron or particle beams [electron microprobe analysis which uses small rastered electron beams in the scanning electron microscope (SEM) or the electron probe microanalyser (EPMA), or particle induced X-ray emission (PIXE) which employs a rastered ion beam of MeV energy obtained with a particle accelerator] has also developed into elemental microanalytical and imaging techniques.[4,5]

Until the recent past, evolution of XRF in a similar way into the microanalytical field was hampered because of the difficulties involved in focusing a divergent X-ray beam from an X-ray tube into a spot of small (ideally submicron) dimensions. The development of synchrotron radiation sources and recent advances in X-ray focusing has changed the scene drastically. In what follows recent progress achieved in X-ray analysis as a microscopical tool will be reviewed and its importance for local elemental analysis and materials characterization highlighted.

Historic overview

Basic qualitative and quantitative analytical capabilities of XRF were established in 1913 by Moseley but the first commercial instruments were introduced only at the end of the Second World War. The methodology became a standard multi-element method in scientific and in particular industrial laboratories. Sequential or multichannel instruments were based on the use of an X-ray tube for excitation, Bragg reflection for wavelength dispersive spectral analysis and conventional (scintillation or gas counting) pulse counting detectors for the measurement of fluorescence X-rays. As a result of severe matrix effects the calibration with this method was originally solely based on the use of reference samples with a very similar composition to that of the unknown, hence the areas of application were in quality control of start-or-finished products in metallurgy, the polymer industry, ceramics and in research areas such as the routine analysis of, for example, soils, rocks and minerals.

The XRF methodology became more versatile and, hence, more generally applicable, in its quantitation for multi-elemental analysis with the advent of energy dispersive XRF (EDXRF) around 1970. The semiconductor diode as an energy dispersive detector is able to measure the entire energy spectrum simultaneously, although with a resolving power for the X-ray spectrum such that computer based deconvolution methods are required to obtain net intensities of individual X-rays.[6] In contrast to wavelength dispersive detection based on Bragg reflection, the measurements in EDXRF are more efficient as the detector can be placed closer to the sample and the equipment is mechanically simpler.

In the last 10–15 years, grazing incidence or total reflection XRF (GXRF or TXRF) has been developed as an analytical method for ultratrace determinations from solutions and dispersions and for surface analysis directly on a solid sample. In addition, by scanning around the reflection angle it developed into a tool for materials science, allowing measurement of density, roughness and layer thicknesses[7,8] and depth profiling.

X-ray microanalysis

The microscopical equivalent of the conventional bulk XRF technique (μ-XRF) is currently subject to rapid evolution. In this methodology, analysis is based on the localised excitation of a microscopically small area on the surface of a large sample or the bulk analysis of a microscopically sized object. The

† Presented at the XXX Colloquium Spectroscopicum Internationale (CSI), Melbourne, Australia, September 21–26, 1997.

Table 1 Characteristics of different microanalytical techniques

Technique*	Projectile	Quantum energy/ keV	Destructive?	Spot size/ μm	Penetration depth/ μm	LLD† (ppm)	Accuracy (%)
SIMS	Ions	10–30	Yes	<1	0.010	<1	>10
LMS	hν (UV)		Yes	~1	1	~1	>50
μ-PIXE	Protons	$2–3 \times 10^3$	Yes/no	0.3	5–100	5–10	10
EPMA	Electrons	5–100	No	<0.1	1–5	>100	>20
μ-XRF	X-ray	10–50	No	3–15	10–1000	1–100	5

* SIMS = secondary ion mass spectrometry; LMS = laser microprobe mass spectrometry; PIXE = particle induced x-ray emission; EPMA = electron probe microanalysis. † LLD = lower limit of detection.

sample is translated through the beam in a raster movement for imaging applications (Fig. 1). The rationale for this development is several fold as there are a number of intrinsic advantages of the application of XRF as a microscopical tool.

1. The complex but well understood interaction of X-rays with matter allows for quantitative analytical results to a degree which is lacking in most of the other microscopic analytical methods.

2. In contrast with most other beam methods, high energy photons can penetrate deep below the surface of materials and more readily provide data on the bulk sample composition.

3. X-ray imaging can be done in an air environment on large samples and requires little if any sample preparation. Non-conducting samples can be analysed without problems and X-ray irradiation causes a lower thermal loading or radiation damage than most other techniques, allowing the non-destructive analysis of sensitive or valuable materials.

4. X-ray equipment is simple in construction in comparison with that of scanning particle beams (at least if one does not take into account the primary radiation source and more involved focusing tools).

The rapid evolution of μ-XRF was triggered by two concomitant technological breakthroughs.

1. The availability of relatively simple and cost-effective devices for obtaining a small dimension X-ray beam such as, *e.g.*, capillary optical devices. This development paved the way for the exploitation of microscopic XRF analysis in the laboratory environment using conventional laboratory X-ray sources (X-ray tubes).

2. Developments in synchrotron storage ring technology, insertion device design and X-ray optics providing polarized photon beams with unprecedented intensity and brilliance on a microscopical area. The growth in achievable brilliance as a function of time is illustrated in Fig. 2 and this growth is compared with (considerable) advances in supercomputer calculating power (adapted from Williams).[9]

The brilliance achieved and subsequently the radiation flux incident on the sample is directly responsible for the sensitivity of XRF and related methods as a microscopic tool. Hence, over the past few years, X-ray methods for chemical analysis have evolved from a bulk analytical technique to a sensitive and accurate micro-analytical tool that, taking into account the sensitivity and accuracy of analysis achieved, readily complements or surpasses other available instrumental micro-analytical methods.

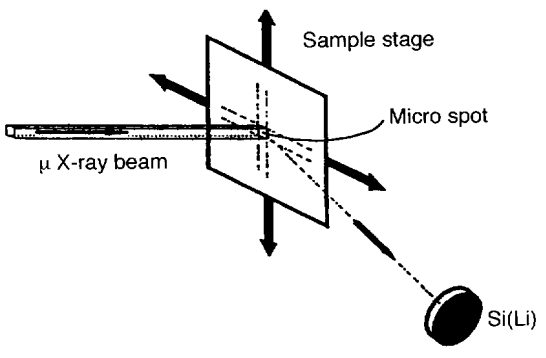

Fig. 1 Schematic representation of XRF.

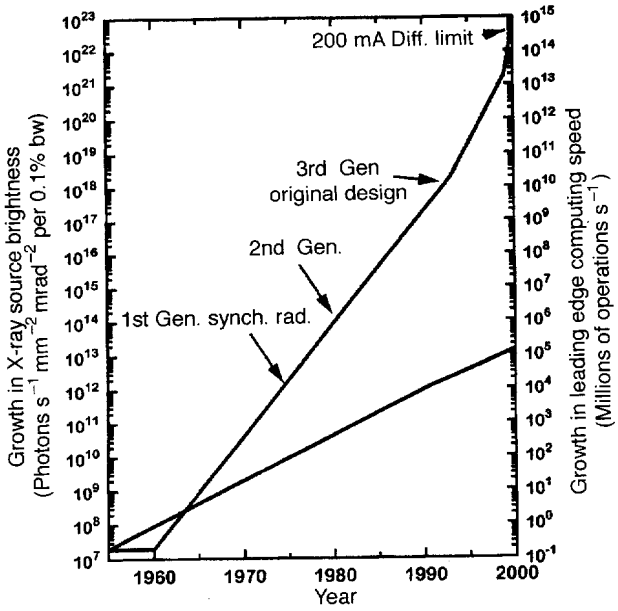

Fig. 2 Growth of achievable brilliance as a function of time; comparison with supercomputing power (adapted from Williams, ref. 9).

Quantitative analysis

Most methods considered in Table 1 (EPMA, scanning Auger microscopy, dynamic and static SIMS, *etc.*) cannot be considered as accurate methods of analysis except in the case of unrealistically simple systems. Their application relies on the use of certified reference materials, which with very few exceptions, are not available. The reason for this is the absence of reliable quantitative methods of analysis at the microscopic level. Hence, the world of microanalysis is badly in need of at least one method able to act as an accurate reference and a validation tool for the other microanalytical techniques. It will be demonstrated that μ-XRF is a possible candidate for validation of the results of other methods and for certification.

According to its present reputation, XRF is considered a poor method for any certification purposes due to intense matrix effects (by primary and secondary radiation X-ray absorption and secondary fluorescence). These effects mean that in, *e.g.*, the WDXRF technique, reliable results can only be obtained through calibrations with a set of standards of closely similar composition to the unknown samples. Its past (and present) attractiveness results from its applications as a process control tool for repeated analyses of series of samples with closely matching radiation absorption/enhancement effects. Energy dispersive XRF also suffers from a number of

drawbacks (spectral overlap, poor statistics, *etc.*), although, when the method is exploited with nearly mono-energetic excitation radiation from, *e.g.*, a secondary target set-up, the corrections for matrix effects become more manageable.

On the other side, the physical basis of the interaction of X-rays with matter is fully understood and the physical constants governing the interaction and radiation absorption are well-known as a result of metrologically sound measurements. In principle, it is certainly possible to correct fully for deviations of linearity between measured intensities and elemental concentrations, provided that time and effort are spent to make the proper (iterative) calculations or to apply Monte Carlo type of simulations.[10,11] This is definitely true in analytical conditions where the set-up is simplified as much as possible (by the use of monochromatic primary excitation with a solid state energy dispersive detector on a sample with a well characterized shape and surface condition). Hence, despite its poor record so far as a quantitative macroscopic analytical tool, XRF has much potential as a method for microscopic elemental analysis. Indeed, in this case, absorption and secondary fluorescence effects are virtually absent or can be adequately corrected for. Even for inhomogeneous and irregularly shaped objects, XRF analysis is, in a number of cases, able to make a distinction between chemical compositional variation and sample topological effects.[12]

Other methods for microanalysis, such as X-ray photoelectron spectroscopy (XPS) or scanning Auger spectrometry and scanning microscopy (AES, SAM) are more difficult to apply as quantitative tools as they require an understanding of the change in energy distribution of electrons as they move in solids. In contrast to XRF, in these last methods the interaction of the microbeam occurs with the electron cloud of outer electrons instead of with the core electrons and these are more dependent on the chemical environment of the analyte atoms. Nevertheless, as was demonstrated in a recent review of qualitative analysis with XPS by Tougaard,[13] principles and rules of general validity ('universal' cross sections) can be defined which give a reasonably accurate description of the inelastic scattering process and open the way for reasonably accurate quantification. Next to the quasi non-destructive methods based on electron and X-ray microbeams, highly sensitive but destructive methods such as static and dynamic SIMS are, if applied to complex systems, not better than semi-quantitative tools, unless extreme efforts are invested in the calibration of the instrument and one limits oneself to an extremely narrow range of investigated materials.

Considering all this, XRF set-ups can be considered to be able to assist other microanalytical methods in their attempts towards accurate quantitative analysis and may become a tool for application as a reference method for elemental trace analysis on the microscopic level.

INSTRUMENTATION

X-ray tubes

Until the advent of synchrotron radiation (SR) sources, the conventional X-ray tube was the source for all analytical applications. Through irradiation with energetic electrons on the anode, X-ray tubes produce a continuum of X-rays with the target fluorescent radiation superimposed on it. Its output intensity has remained virtually constant over the years (the horizontal line in Fig. 2) as the limit imposed on X-ray intensity is the heat dissipation from the anode upon impact of the energetic electron beam. Radiation is emitted quasi-isotropically from the area of impact of the electron beam. Conventional wavelength dispersive analysers and energy dispersive analysers with secondary targets use tubes capable of operating up to 3–4 kW. Low power tubes (< 100 W) are most common in the direct excitation instruments often applied in energy dispersive analysis. Rotating anode tubes more efficiently remove heat from the impinging electron beam and can be exploited up to a power of 18 kW.

Wavelength dispersive XRF relies on the use of the energy spectrum containing Bremstrahlung and characterictic radiation from the anode (Mo, W, *etc.*) whereas in the majority of EDXRF applications, excitation with the fluorescence spectrum of the anode or a secondary target are considered to be the most sensitive and reliable source as this leads to a reduced background continuum. The X-ray source area can be dimensionally confined through the focusing of the electron beam by means of a Whenelt cylinder or even more sophisticated focusing technology, also employed in electron microscopes.

One simple way of producing a spatially confined X-ray beam from an X-ray tube consists in collimating the radiation cone that emerges from the X-ray tube with suitable apertures. Several types of X-ray tubes can be used for this : low power (*ca.* 100 W) air cooled tubes with an electron beam microfocus anode, high power (1000 W) water cooled tubes and rotating anode tubes (typically 10 000 W). These sources are exploited with or without spatial confinement of the electron beam to decrease the spot from which the secondary radiation is produced and, hence, increase the brilliance.

In the late 1980s systems based on low power (50 W) microfocus type X-ray tubes were developed which showed imaging potential with a lateral resolution in the range of a few tens of μm. The commercial system of Kevex[14,15] had a beam size at the anode of 250 × 250 μm and further collimation on the sample was achieved with variable size pin-holes of 30–100 μm, allowing stepwise scanning over a sample. The limited photon flux intensity, resulting from collimation of the X-rays severely compromised the obtainable elemental sensitivity. As a result, commercial instruments only recently succeeded in making a real breakthrough in the analytical instrumentation market.

In view of the large distance between the X-ray anode and the collimation apertures and the subsequent loss in intensity, new approaches were needed to obtain a more intense X-ray beam on the sample. Next to improving the geometry of the X-ray tube itself, there are two ways of doing this: (*i*) resorting to some type of focusing of the X-ray beam, this is the only approach which can be used with laboratory instruments; or (*ii*) the 'brute force' approach of increasing the X-ray source intensity by resorting to the use of the intense radiation flux of storage rings in parallel with recent advances in X-ray microfocusing. Both approaches will be reviewed later.

Synchrotron radiation sources

When electrons or positrons with relativistic speed are confined in a continuous quasi-circular path comprising straight sections and bent sections (in so-called bending magnets) in which they are forced to change direction, electromagnetic radiation is produced. This radiation produced at the bending magnets is *ca.* 10^6 times as intense as that produced in conventional X-ray tubes and extends continuously over a considerable energy range from the IR to the hard X-rays (white beam). The characteristic energy of the radiation, defined as the median of its power spectrum, is given by $2.218E^3/R$ where E is the energy of the orbiting particles in GeV and R is the radius of curvature of the beam orbit at the ending magnets in m.

When comparing radiation sources it is necessary to consider in addition to the flux, F, (number of photons per energy interval) also the brightness, B, (the emitted flux per solid angle) and the brilliance, b, (the brightness per unit source area). For a collimated beam made by, *e.g.*, a pin hole, the flux at the sample is proportional to the brightness. When optical devices are used to obtain an image of the source it is the brilliance that is the relevant parameter for the flux density at the focus position.

A particular advantage in comparison with the conventional X-ray sources is the extremely high brilliance achieved with synchrotron radiation (SR) sources. The brilliance is expressed as the number of photons emitted per unit source area over a unit angle of emission and per unit energy (photons s^{-1} $mrad^{-2}$ mm^{-2} per 0.1% of radiation bandwidth, *e.g.*, per 1 eV at 10 keV). In addition, in the plane of the storage ring the radiation is linearly polarised with the *E*-vector parallel to the ring plane and the *B*-vector normal to it. The radiation is highly collimated along a direction tangential to the movement of the electrons in the ring, which facilitates the delivery of the radiation to a predefined sample area.

The high intensity and directionality implies that SR is ideally suitable for the generation of X-ray microbeams of microscopic dimensions in synchrotron XRF (SR-XRF). The polarization of the incident radiation can be used to reduce the relative contribution of scattered radiation reaching the detector as scattering cross sections are dependent on the polarisation whereas the photo absorption cross sections (and hence the production of fluorescence radiation) are not. Shown in Fig. 3 is the difference in peak-to-background ratios achieved in an EDXRF spectum collected from a polypropylene standard in a geometry that takes advantage of the polarisation (measurement in the plane of the storage ring, degree of horizontal polarization estimated at $P=98.7\%$) in comparison with a measurement in which the detector is positioned out of the plane of the storage ring.[16,17]

In addition, thanks to the high directionality of the beam, quasi-monochromatic X-ray microbeams can be generated from the white spectrum through the use of X-ray monochromators. By tuning the energy of the source, the strong energy dependence of the inner shell photo-electric cross sections can be exploited to increase the sensitivity of selected elements selectively or to obtain chemically significant results [as is done in X-ray absorption spectrometry (XAS), extended X-ray absorption fine structure analysis (EXAFS) and X-ray absorption near edge scanning (XANES)].

With these characteristics it is not surprising that a number of existing storage rings have been employed in μ-SR-XRF experiments combining the advantages of XRF as an elemental analytical tool with the unique possibities of SR.

Most of the presently operational SR sources belong to the so-called second generation facilities, to distinguish them from the first generation ones in which the SR was produced as a parasitic phenonom in high energy collision experiments with elemental particles. They were essentially designed to exploit the radiation produced from the bending magnets. Of special significance for future activities are the new so-called third generation storage rings, which are specifically designed to obtain unprecedented intensity and brilliance. A number of these are operational at present: the European Synchrotron Radiation Facility, ESRF, Grenoble, has been in operation since the end of 1994; more recently available is the Advanced Photon Source, APS, Argonne, IL, USA, while the SPring-8 storage ring, located in Harima, Japan is nearing completion.[17–19] Compared to second generation rings these new storage rings are characterized by their high energy of 6–8 GeV, hence the hard (energetic) X-rays they produce. Also significant in these devices is the systematic use of insertion devices that are placed in the straight sections of the storage ring (wigglers and undulators). Wigglers are magnetic structures that create multiple oscillations of the orbiting particles around the beam path and hence increase both the energy and the intensity of the radiation. Undulators are designed to create smaller and more frequent deflections, giving rise to interference effects in the radiation produced, yielding coherent radiation concentrated around several specific energies (harmonics). In addition, X-ray optics of increased sophistication amplify considerably the flux and brilliance. In ESRF the design goal was a brilliance from an undulator of 10^{18} photons s^{-1} μm^{-2} $mrad^{-2}$ per 0.1% bandwidth. In actual practice 10^{20} is achieved at present on the first harmonic of the standard ESRF undulator source.

At all three of the above mentioned third generation rings, instrumentation for XRF microprobe analysis and related methods (microdiffraction, tomography, imaging, edge absorption, XANES, EXAFS, *etc.*) are planned or under development at present,[20–22] mostly using undulator sources.

In further sections of this paper analytical applications performed at some second generation facilities and the ESRF third generation instruments will be discussed in more detail.

Production of microscopic X-ray beams

Refraction of X-rays and total reflection

Refraction of X-rays exploits the situation that the real part of the complex index of refraction of matter is somewhat smaller than unity compared with the index in vacuum (or air) where it is equal to 1:

$$n=1-\delta-i\beta \qquad (1)$$

where β is the absorption index and δ, the refractive index decrement is typically between 10^{-5} and 10^{-7}.

Refractive lenses, although they are extensively used in visible-light optics, have until recently never been considered

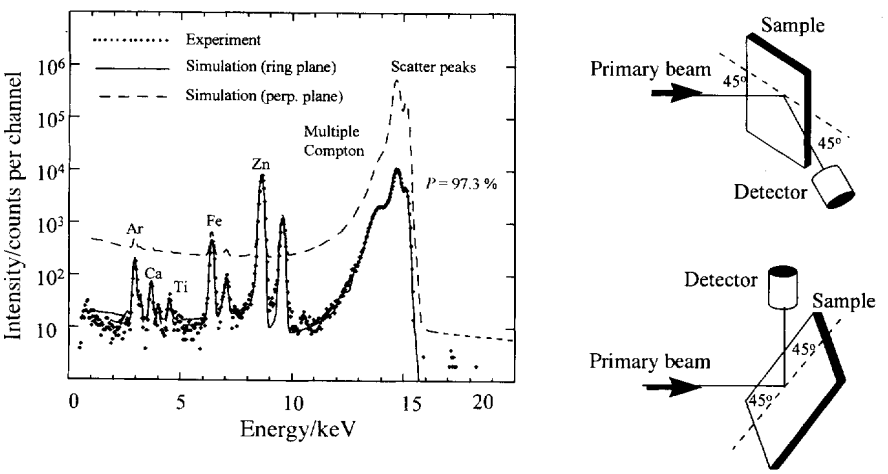

Fig. 3 X-ray spectra obtained from 1 mm thick polypropylene film with measurement in the horizontal ring plane (degree of horizontal polarization *ca.* 99%) and with measurement out of the plane of polarization. Experimental points as dots; full lines calculated spectra with Monte Carlo simulation.

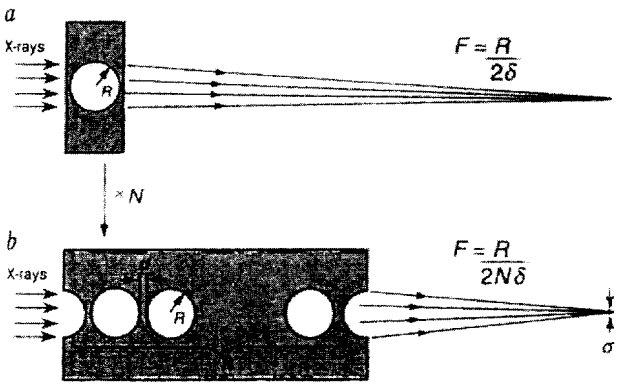

Fig. 4 Schematic principle of X-ray focusing by compound refractive lenses. Single lens consisting of spherical hole in material (*a*); a compound lens consisting of a number of consecutive holes with decrease of focal length (Snigirev *et al.*, ref. 23).

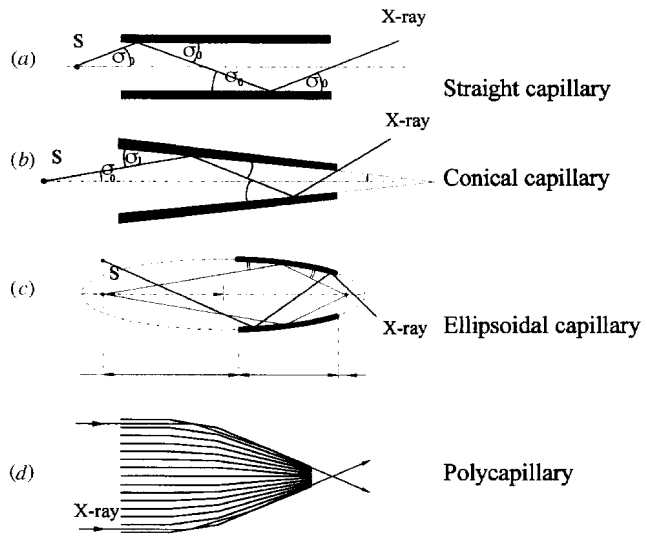

Fig. 5 Schematic of capillary beam confinement systems: straight capillary, conical capillary, ellipsoidal capillary and polycapillary system (Kurnakhov lens).

for X-rays because the refractive index (eqn. 1) is so small (which would make the focal distance extremely long) and because absorption dominates. In contrast to focal lenses for visible light an X-ray refractive lens must be concavely shaped as the term $(1-\delta)$ is smaller than unity.

A breakthrough in simple refractive lens technology was achieved recently by Snigirev *et al.*[23] The design of a simple compound lens system fabricated by drilling a number of cylindrical holes in a low Z material (*e.g.*, Al) is shown in Fig. 4. The array of N holes focuses the radiation from a parallel beam at a focal line which is N times shorter than the extremely long focal distance for a single hole. Such a lens system is cheap and easy to make but suffers from the disadvantage of X-ray scattering in the aluminium mass. More complicated designs with other construction materials such as carbon or beryllium have shown that focusing in both dimensions can be readily achieved and that the drawbacks in its use can be effectively overcome. It has been shown that two-plane refractive lenses have a strong potential for further optimization of the undulator beamlines of ESRF, increasing the spectral flux per unit surface without affecting considerably the brilliance and divergence of the beamline.[24]

As defined from Snell's law there exists a critical angle of incidence, θ_C, for which total reflection conditions occur when radiation is directed to a flat surface. The angle inside the material is then equal to zero. When defined in practical units, θ_C:

$$\theta_C = 99.1 \times E^{-1} \times (Z\rho/A)^{0.5} \qquad (2)$$

with θ is in min of arc, ρ is density and Z and A, atomic number and relative atomic mass, respectively; *e.g.*, for hard X-rays at 10 keV on a silicon reflector, θ_C is about 3 mrad or 0.2 °.

The reflectivity ratio drops sharply from unity to zero around the critical angle and is density dependent. The penetration depth of the radiation is independent of the energy of the primary beam and can be as low as a few nm.

Refraction in these grazing angle irradiation conditions is used in several applications, one of them being TXRF; another application of this principle is in the area of X-ray focusing.

Capillary optics for X-rays

Grazing angle refraction of X-rays can be used for the confinement of X-rays using multiple reflection in a glass capillary. Capillary optics are rapidly developing as an impressively simple tool for obtaining a small X-ray beam from a larger beam. They operate through single or repeated total reflection of X-rays at the inner wall of a glass capillary tube.[25]

Three major types of capillary X-ray concentrators can be distinguished. The most simple is the straight capillary [Fig. 5(*a*)]. During the repeated total reflection of the X-rays at the inner walls of a glass tube, the angle of incidence, θ_o, in this case remains constant. Thus straight capillaries act as waveguides and are used to transport X-ray photons from, *e.g.*, near the anode of the X-ray tube to the sample. In this way they partly eliminate the $1/r^2$ losses that would occur when using a collimator. In order to increase the photon flux further, it was attempted in the late 1980s to use these glass capillaries as X-ray concentrators. Conically shaped capillaries with a taper angle (squeeze the radiation down to the dimensions of the end diameter as can be seen in Fig. 5(*b*), but upon each reflection the reflection angle increases by an amount 2γ and only photons for which an angle of incidence, θ_N, of the last reflection is smaller than the critical angle θ_C will be transmitted by the capillary. Upon leaving the capillary the photons may travel in all directions with $\theta_N \leqslant \theta_C$, hence, the emerging beam has a divergence of the order of θ_C. The capillary thus acts as a concentrator producing a small, intense beam at the expense of divergence. Hence, the beam is smallest at the capillary tip and the sample should not be placed too far away from it. In practice, for a 1 μm beam size the optimum working length amounts to *ca.* 100 μm.

A more recent development is the ellipsoidally shaped capillary tube shown in Fig. 5(*c*). Here photons orginating from a focal point S in the ellipse are refocused on a point on condition that they undergo only one single total reflection. The others behave in a similar manner as in a conical capillary. The X-ray beam generated by such a device therefore consists of two types of contributions: a 'first order' component which converges towards the focal point and a 'higher order' component that is strongly divergent. The production of such devices is a recent development and applications are still scarce but the potential is considerable.

Curved bundles of many (hundreds to several thousands) glass capillaries (polycapillaries or Kumakhov lenses) [Fig. 5(*d*)] can be used as devices that are more compact in length than the single capillaries. These lenses can effectively transform a divergent beam into a quasi-parallel beam, focus radiation, turn it through relatively large angles and cut off the hard part of the spectrum. The focal spot can be displaced farther away from the tip than in the monocapillaries but these devices cannot achieve the small spot sizes of the monocapillaries.[26]

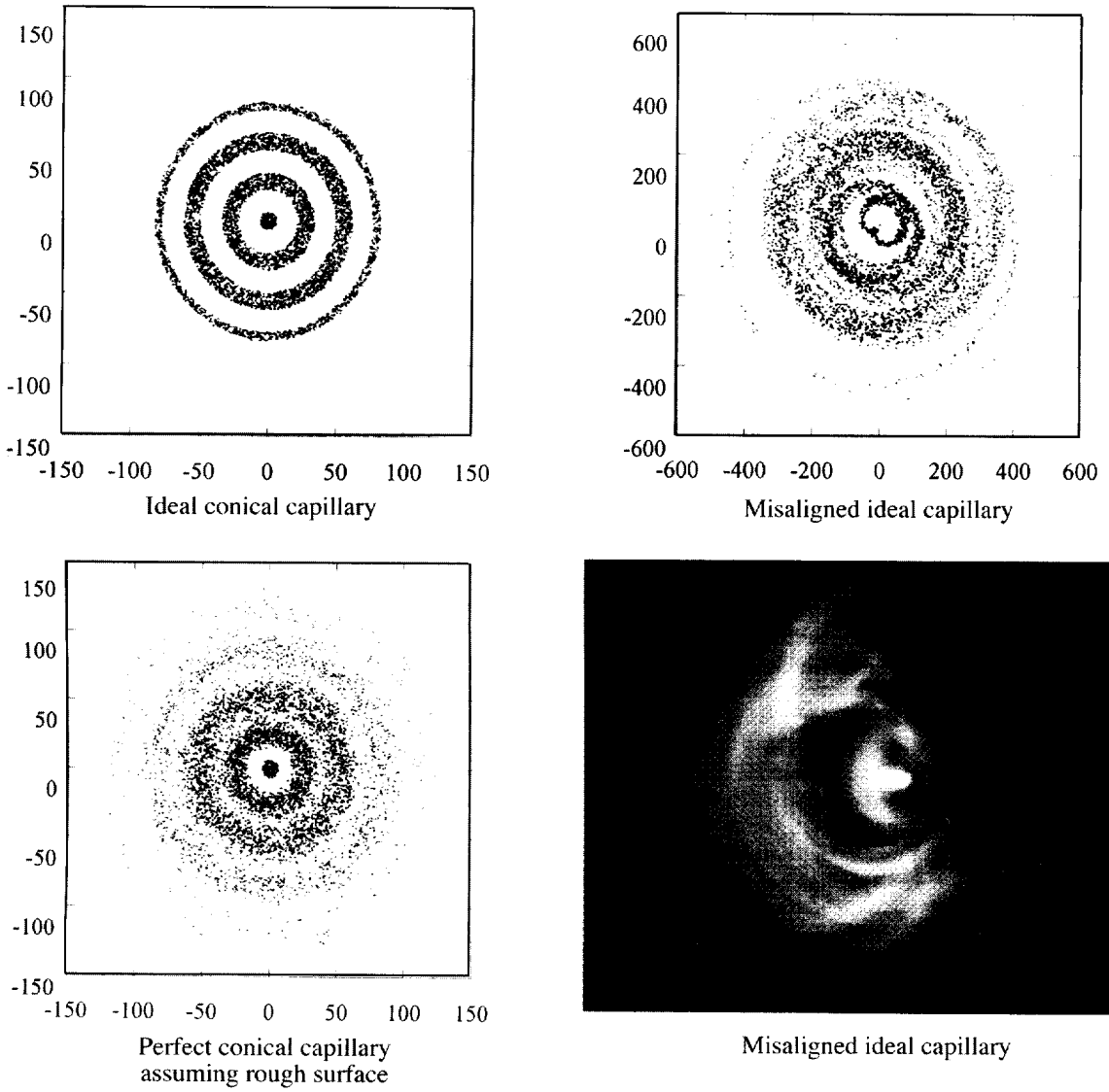

Fig. 6 Simulated X-ray intensity distributions obtained by Monte Carlo ray tracing methods on: an ideal capillary; a mis-aligned capillary; a capillary with a surface roughness of 300nm. Experimentally measured intensity distribution (Engström *et al.*, ref. 27). All numbers are in μm.

In principle, capillaries create a beam whose size is determined by the inside diameter of the end of the glass tube and not by the X-ray source size or optical aberrations. In fact when applying a real monochromatic point source to them the individual rings representing different refraction orders will become visible. In theory, tapered capillaries of a parabolic inside surface shape are fairly effective devices for condensing the radiation down to a small size. In practice, it is difficult to achieve this ideal shape, but this effectively reduces only the throughput (resulting in a loss of brilliance) not so much the exit beam size, which remains equal to the inside diameter of the tip of the capillary. As the critical angle varies inversely with the photon energy, the gain (X-ray flux per unit area) is energy dependent.

Next to the obvious parameters such as the shape and dimensions of the capillary, other factors determine its performance such as the material the capillary is made of, its surface roughness and the radius dependence as a function of length. Any experimental characterization of a capillary device must be performed in parallel with some kind of ray-tracing calculation.[27] Shown in Fig. 6 are simulated spatial intensity distributions from a well aligned 'ideal' capillary and a mis-alligned capillary as obtained by Monte Carlo simulation calculations. Also shown in Fig. 6 is what happens when a capillary with a surface roughness of 300 nm is introduced and the symmetric rings represent different reflection modes as halos around a central spot. The experimentally obtained distribution for a real misaligned capillary is also shown.

Owing to absorption, the reflectivity below θ_c is higher for a low atomic number than a high atomic number material. Therefore, boron silicate glass is mostly used rather than, *e.g.*, lead glass, although θ_c for this material is considerably higher [see eqn. (2)].

Other X-ray focusing devices

Capillaries are only one of the many possible optical elements for X-rays. Other devices, which are, in practice, mostly used in SR sources but also have been incorporated in conventional X-ray sources are bent crystals and multilayer X-ray mirrors. Several monochromator–focusing designs are used in practice such as bent mirrors in the Kirkpatrick–Baez geometry. These cannot always achieve the microscopic focusing level required and need to be combined with other demagnification tools for real microscopic X-ray probes such as the glass capillaries discussed previously. Other possibilities are Fresnel and Bragg–Fresnel zone plates made by electron beam lithography, optical lithography or ion beam etching techniques.[28,29] They consist

of concentric opaque rings in which photons are diffracted as they pass through the gaps between the rings and lead to a well defined focal spot with high flux and good signal-to-noise ratio. These devices combine the functions of diffraction and focusing, acting simultaneously as monochromator and focusing lens with a focus of considerably less than 1 μm^{-2}. Bragg–Fresnel lenses are well suited for focusing radiation emitted by undulator sources.

MICROFLUORESCENCE IMAGING TOOLS

The extent to which these optical devices can be used for the construction of laboratory and synchrotron based μ-XRF instruments will now be discussed.

Laboratory μ-XRF instruments

Early designs were based on low power X-ray tubes providing a small spot fitted with 10–100 μm apertures and were adapted to give commercial instruments. Pella and Feng[30] reported on the analysis of coarse environmental particles with a diameter between 50 and 200 μm and on the problems associated with quantification of these heterogeneous samples and the development of angorithms for quantitative analysis. Boehme[31] used a system for quantitative mapping of geological materials.

At present, several manufacturers are commercialising μ-XRF instruments with a high power, focus type X-ray tube that are based on the use of conical capillaries, giving 5–10 μm spot size and rapid scanning and compositional mapping capability with ppm detection limits (*e.g.*, Horiba, EDAX, XCO, a small company from Sweden).

The total reflection angle is small and energy dependent, *e.g.*, for glass at 10–20 keV it is 5–10 mrad. Acceptable fluxes of X-rays confined to cross-sections in the range of 4–100 μm could thus be obtained,[32–34] allowing analytical applications in both X-ray diffraction and fluorescence analysis with 0.01–10 pg detectable amounts.

In general μ-XRF fills the gap between conventional bulk XRF and high resolution electron probe microanalysis. Count rate limitations impose long counting times for each individual pixel, hence, collection of an image by point-by-point irradiation remains a time-consuming process.

University of Antwerp μ-XRF instrument

A laboratory scale μ-XRF instrument based on a rotating anode X-ray generator and source and various types of capillary concentrators was constructed at the University of Antwerpen and will be briefly described. A more detailed description is available elsewhere.[35] It consists of a Siemens M18XHF rotating anode X-ray tube of the direct drive type in which a copper or molybdenum cylinder is directly fixed on the rotor of a small internal electromotor to minimise vibrations and noise. X-rays are created with a different spot size through the use of a Whenelt cylinder for electron beam focusing. At a power mode of 12–18 kW a spot of dimensions $0.5 \times 10\ mm^2$ can thus be obtained. The distance from this point to the Be window of the tube is 6.0 cm. Glass capillaries are contained in a cylindrical brass holder mounted on a five axis gimbal lens holder which allows for precise positioning of the capillary in the beam. The entrance of the glass capillary can be positioned to within 7.0 cm of the X-ray source. Samples can be mounted on a stage with *XYZ* controlled to within 1 μm and rotation to within 0.01°. The fluorescence radiation is detected with a $80\ mm^2$ Si(Li) detector with 180 eV resolution for Mn Kα and can be shielded with 4–8 mm molybdenum apertures. Normally, the detector is placed at 90° to the incoming beam and at 45° to the sample; under these conditions the closest sample–detector distance is 13 mm. A schematic drawing of the set-up is shown in Fig. 7.

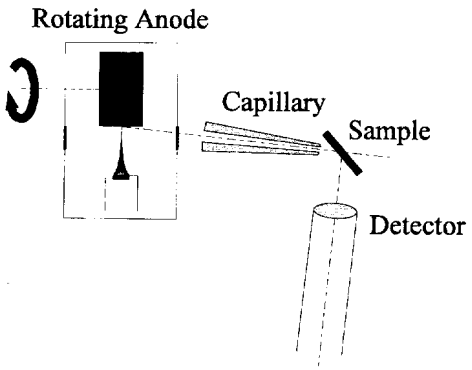

Fig. 7 Schematic representation of a rotating anode capillary optics microfluorescence spectrometer (Janssens *et al.*, ref. 35).

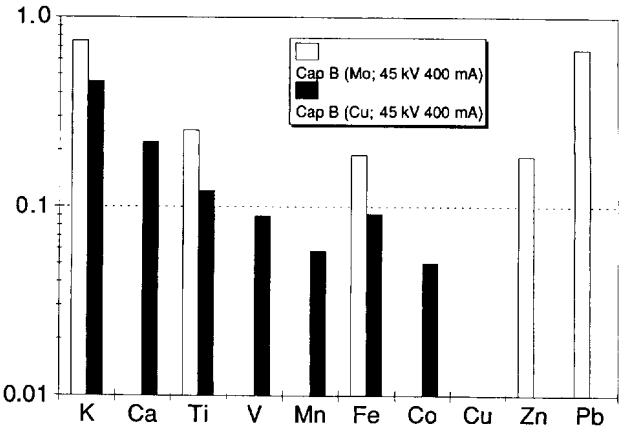

Fig. 8 Absolute detection limits obtained for the microfluorescence system of fig. 7 (Janssens *et al.*, ref. 35).

Spectrum acquisition, sample scanning and spectrum evaluation through non-linear least squares fitting are processed through a dedicated PC.[36] The focusing characteristics of several single capillaries with various inner diameter profiles as well as polycapillary lens systems were tested in this system both by experimental measurements and ray-tracing. They yielded count rates of about 500 000 counts s^{-1} at 18 kW and spot sizes of about 15 μm at a realistic capillary–sample distance of 1 mm. The minimum detectable amounts for several elements obtained with two capillaries are shown in Fig. 8.[35]

The capillaries act as a high energy filter because θ_c drops with X-ray energy capillaries, and, in addition, surface roughness at the inner capillary walls reduces the reflectivity more at higher energies. It appears that at 10 μm lateral resolution the 10 ppm level is possible provided that sufficiently long counting times are employed.

SR X-ray microbeam instruments

Micro SR-XRF spectrometers can be assembled in different ways using components such as mechanical collimators, monochromators selecting a particular energy from the white beam by Bragg reflection and flat mirrors to deflect the beam and to remove high energy photons and curved mirrors to focus the beam. The sample is moved with respect to the beam on a motor-driven stage.

The characteristics of a number of SR-XRF instruments currently in operation at various synchrotron laboratories using bending magnet beamlines are listed in Table 2. Most major synchrotron laboratories have a dedicated or partly dedicated SR-XRF facility, although microscopic analysis is

Table 2 Characteristics of currently operating X-ray microprobes

Storage ring	E_c/ keV	Spot size/ μm^2	Energy/ keV	Optical system
DCI	1.9	N/A*	8–20	Curved graphite crystal
		2 × 2	10	Bragg–Fresnel lens
Hasylab	31.7	3 × 3	White	Pinhole
		?	White	Conical capillary
NSLS	5	5 × 5	White	Pinhole
Photon Factory	1.9	3 × 10	10	Wolter
SSRL	2.0	3 × 3	10–20	Kirkpatrick–Baez
VEPP-3	5.4	N/A	10–60	Channel-cut monochrometer

* N/A, not applicable.

not possible at all sites. Also, very diverse optical arrangements are employed ranging from simple pinholes (collimated white beam excitation) to focusing monochromatic optics. A number of the optical systems mentioned in Table 2 have only very recently been tested in practice and the analytical qualities of the corresponding SR-XRF spectrometers still need to be evaluated.[36]

Two typical configurations relying on capillary (Hasylab, Hamburg, Germany) or pinhole [NSLS, (National Synchrotron Light Source), Brookhaven, NY, USA] generated microbeams as used at the second generation rings are shown in Fig. 9.[38] Other specific optical systems are listed in Table 2.

Focusing of the SR X-ray beam can be achieved by other means. Circular or linear Fresnel zone plate lenses with features as small as 50 nm have been demonstrated to give submicron spots.[39]

All currently operating μ-SR-XRF stations employ different optical configurations for producing the microbeam. In some instruments, a collimated polychromatic beam is used, an example is the NSLS microprobe. At other facilities (such as the Synchrotron Radiation Source, SRS, Daresbury, UK) focused monochromatic radiation is employed. A monochromatic microbeam has the advantage that very high peak-to-background ratios can be obtained in the detected X-ray spectra compared with polychromatic white beam excitation. The polychromatic beam leads to efficient excitation and to a high background continuum of scattered radiation. The spectrum obtained for a biological reference sample (NIST SRM 1571, Orchard Leaves) is shown in Fig. 10(*a*). The corresponding spectrum in Fig. 10(*b*) is for monocromatic excitation and was collected at SRS. Except in the region of the (in)coherent scatter peaks, almost background-free spectra can be recorded, where the background is considerably lower than for the white beam excitation. Elements whose characteristic peaks are located just adjacent to the scatter peaks are detected under optimal conditions. At current second generation SR facilities, ppm lower limits of detection (LLDs) for a limited number of elements can be obtained in this way (Fig. 11). If the energy of the radiation can be tuned, selective excitation of otherwise interfering elements (such as Ti–Ba, As–Pb) can be achieved. Calibration of this type of spectrometer is also relatively simple, while the intensity of the scatter lines can be used to estimate the sample thickness and the effective mean atomic number (Z). On the other hand, elements with absorption edges above the excitation energy are not excited [*e.g.*, Sr, in Fig. 10(*b*)] while for lighter elements the excitation efficiency decreased rapidly resulting in a strong variation of the LLDs with Z, as shown in Fig. 11 (hollow symbols).[37]

Polychromatic forms of excitation have the advantage that (nearly) all elements in the sample are excited with comparable efficiency. Accordingly, a more uniform spectrometer response over the Z range is obtained (see Fig. 11, hollow symbols). This type of excitation is more appropriate for a general materials characterisation instrument. Since no losses in flux occur due to monochromatisation, the elemental efficiency of

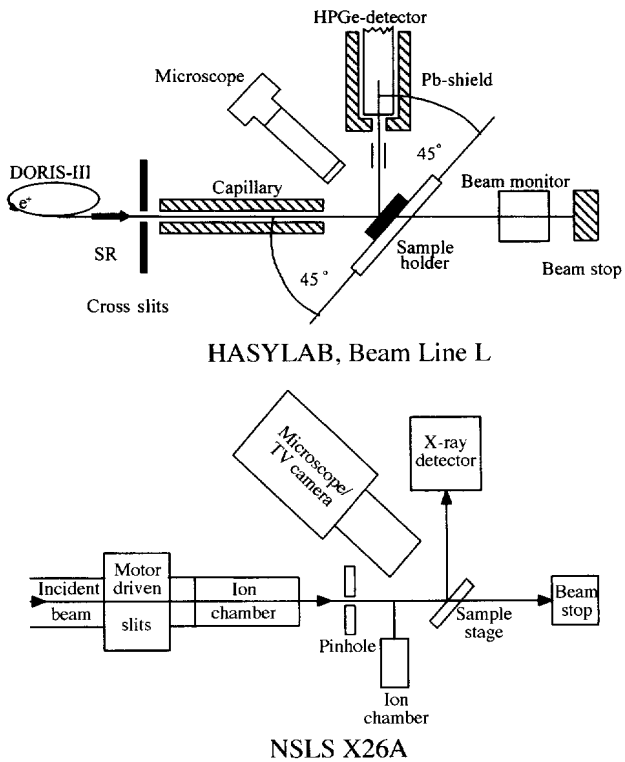

Fig. 9 Experimental arrangement at two second generation synchrotron facilities: top, Hasylab, Hamburg, Germany; and bottom, NSLS, Brookhaven, NY, USA.

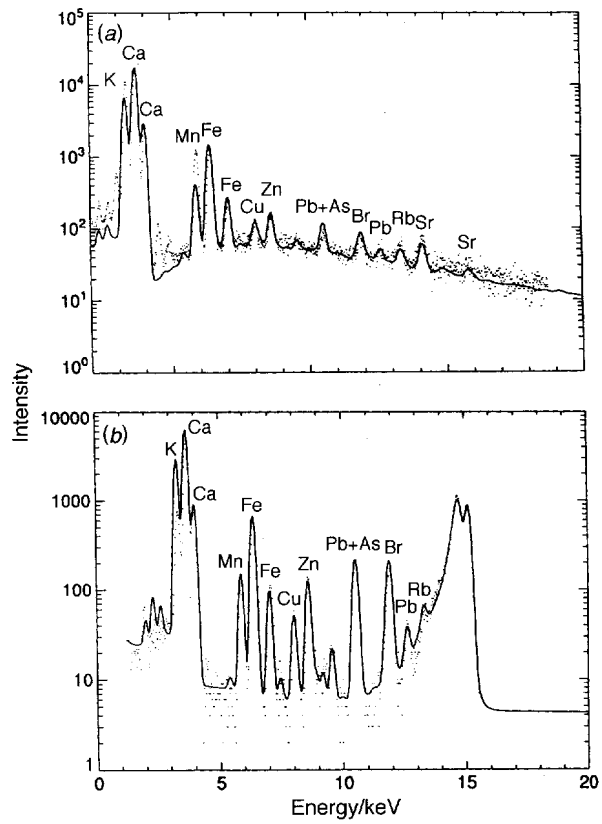

Fig. 10 SR-XRF spectra of biological sample NIST SRM 1571 Orchard Leaves measured with (*a*) a polychromatic source (NSLS) and (*b*) a monochromatic X-ray microprobe (SRS, Daresbury, UK).

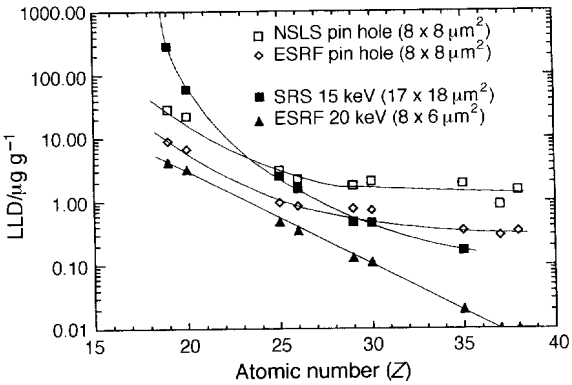

Fig. 11 Detection limits of biological matrix (NIST SRM 1571 Orchard Leaves) in different configurations: NSLS, SRS and ESRF (at a bending magnet).

these set-ups is also higher than when monochromatic excitation is used [compare Fig. 5(*a*) and (*b*)]. On the other hand, quantification of the detected X-ray intensities is more complicated and error-prone. Also, the scattering of the white spectrum in the sample causes a significant background continuum to be present in the EDXRF spectra, as illustrated in Fig. 5(*a*). At current white beam facilities, in routine practice, LLD values in the 1–10 ppm range are routinely achieved.

For monochromatic excitation in SR-XRF it is possible to select a relatively wide energy bandpass (approximately $\Delta E/E = 10^{-2}$) which provides a higher photon flux and lower detection limits compared with a monochromator with a small bandwidth of $\Delta E/E = 10^{-4}$. This is normally achieved with multilayer structures. The application of edge techniques, on the other hand, require the highest achievable bandwidth.

ESRF microfluorescence beamline

At the ESRF a beamline at the undulator insertion device 22 for establishing an XRF microprobe, the microfluorescence, imaging and diffraction beamline (μ-FID$_{22}$) has been completed.[39] The instrument has been operational since autumn of 1997. Before this date limited XRF experiments were possible on the microfocus beamline (BL1, the first operational beamline) at ESRF. This beamline provides micrometer-sized X-ray beams with a flux density of 10^{10} photons μm^{-2} (with a 2 μm focusing capillary) at an energy of 13 keV and with a bandwidth of $\Delta E/E = 10^{-4}$ for simultaneous micro X-ray diffraction (XRD) and micro XRF work. Focusing optics are linear Bragg–Fresnel lenses on a bent crystal and Fresnel zone plates (expected spot size; 1 μm; flux, 10^{11} photons s^{-1}; high energy and for the Fresnel zone plates coherence for holographic application), Bragg–Fresnel in backscattering geometry (<0.5 μm; 10^9 photons s^{-1}; sharp bandpass) and Bragg–Fresnel on multilayer (a few μm; 10^{12} photons s^{-1}; wide bandpass).

A schematic view of this instrument is shown in Figs. 12 and 13.[40] The μ-FID$_{22}$ beamline uses an ESRF undulator in a high β section which provides an X-ray source with a size of 700×35 μm^{-2} and a divergence of 28×18 rad^2 (FWHM) and a brilliance of 4.19 photons s^{-1} $mrad^{-2}$ mm^{-2} for 0.1% bandwidth at 8 keV. A flat mirror and a flat double crystal monochromator are positioned as shown in the layout in Fig. 12.

During the design of μ-FID$_{22}$ the requirements of two types of uses were taken into account. On one side there is an interest in pushing the routine detection capability of μ-SR-XRF to well below the 1 ppm level at the expense of using a microbeam of moderate cross-section (of the order of 5×5 μm^{-2}). On the other hand, there is also interest in

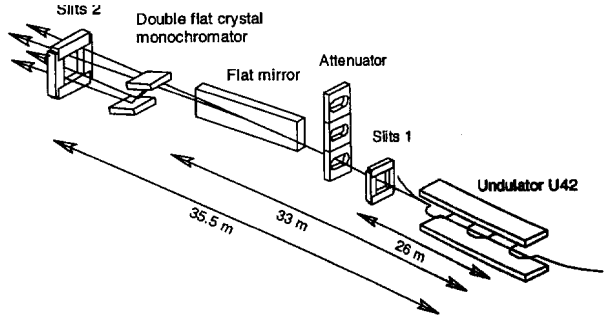

Fig. 12 Main layout of micro-FID beamline of ESRF (ref. 39).

extending the beam dimensions to a sub- μm beam with which a completely new class of samples (*e.g.*, micron sized environmental particles) could be examined with unprecedented lateral resolution, but with a less favourable sensitivity. In order to select optimal configurations compatible with the requirements of both user groups, two end stations are used (experimental hutches I and II). The first is located 40 m from the source with a few micron spot size and 10^{11} photons s^{-1} and the second at 60 m with a submicron spot at 1010 photons s^{-1}. SR-XRF, μ-XAFS (X-ray absorption fine structure), micro-diffraction and μ-tomography will be possible at the micrometer scale.[40]

The energy range of the monochromator is 4–60 keV with a bandpass of $\Delta E/E = 10^{-4}$. The optics are made such that coherence is preserved by polishing the beryllium windows and the optical elements.

When in operation this equipment should combine the quantitative reliability and accuracy of XRF with the sensitivity and the lateral resolution of destructive beam techniques such as, *e.g.*, SIMS.[41]

Operational structure of ESRF

Synchrotron radiation sources such as the ESRF are built and operated to serve a wide user community. The ESRF facility was built in Grenoble, France by a consortium of 12 European nations and provided for the construction of a high brilliance, high energy SR machine with 30 public beamlines constructed mostly on insertion devices. These were selected after wide-ranging consultations of the scientific community. Most of them are or will be operational by the end of 1997 and pertain to areas of research such as materials and surface science, micro-diffraction and crystallography, various aspects of spectrometry, physics, chemistry and biomedicine. With 20% of the time set aside for internal use around 4800 hours per year can be allocated to external users on the basis of projects introduced to review committees. In addition, it is possible for exernal users to build specific beamlines (collaborative research groups, CRGs) at bending magnets to be financed and operated by specific user groups. In return for the use of the facility one third of the availability of the CRG is put at the disposal of the public users.

RELATED METHODS OF ANALYSIS

Besides the elemental analytical capability of XRF, a number of other possibilities for characterization and imaging exist. For some of them, the full potential at the microscopic level has not been fully demonstrated at present.

Total reflection XRF

The TXRF method is based on X-rays incident on the sample at or below the critical angle (or total reflection angle) on an

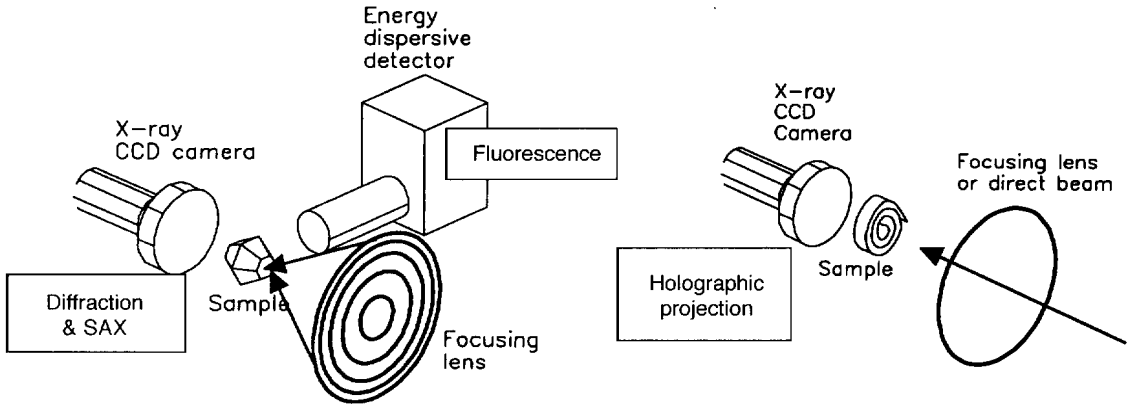

Fig. 13 Experimental set-up for the microprobe applications [XRF and diffraction (left) and for imaging (right); ref. 40].

optically flat sample. The method was developed as an extremely sensitive analytical tool for trace analysis of the surface of solid materials (*e.g.*, semiconductors) or as a tool for determining trace elements in a solution or dispersion brought onto a clean substrate. Hence, TXRF is simultaneously a surface analytical tool or an ultra-trace multi-element tool. Other reviews should be referred to for more details on this method.[42]

Irradiation of a sample with an X-ray beam at an impinging angle below the angle of total reflection conditions gives rise to confinement of the primary X-ray beam to a few tens of nanometers below the surface. The excitation from the top surface layer produces spectra with a much reduced spectral background, thus providing a considerable improvement of the detection limits. Sample material must be available on an optically flat surface reflector, typically a quartz or silicon disk.[42,43] Typical detection limits for TXRF are at the 10 ng level for a 1000 s counting time in conventional instrumentation.[44] Among the many application areas of TXRF, air pollution studies are interesting with reported detection limits for aerosols of the fraction of a ng cm^{-2} and reproducibilities between 5 and 25%. Around 20 elements can thus be detected with detection limits of the order of the ng m^{-3}.[8]

The obtainable sensitivity with laboratory X-ray sources can be increased tremendously by using SR beams.[42]

Chemical state analysis (speciation) using X-ray absorption spectrometry

One of the most exciting new areas of applications of microbeam analysis using SR is X-ray absorption spectrometry (XAS). This technique is based on the irradiation of a sample with a highly monochromatic X-ray microbeam of tunable energy. By scanning the energy over an absorption edge of an element of interest, *e.g.*, the K-edge of Fe in fractional steps and recording either (*i*) the absorption of the beam (absorption XAS), (*ii*) the fluorescence radiation produced (fluorescence XAS) or (*iii*) another shell dependent phenomenon, the fine structure of the edge is measured. The edge location and shape provides information on the chemical environment, as the energy necessary to excite the bound electron shifts slightly with changes in the chemical environment of the chemical species involved.[45]

Two energy regions around the edge may be exploited and provide different structural information. The near edge region (X-ray absorption near edge structure spectrometry, XANES) measures the position of the edge and the presence or absence of pre-edge structure. From XANES data the oxidation and coordination state of the studied atom can be derived. The extended region (extended X-ray absorption fine structure analysis, EXAFS) provides infomation on the number, the atomic number and the distance of neighbouring atoms.

Both variants of absorption spectrometry have up to now been predominantly used in bulk investigations, especially for high technology materials and catalytic studies. The transmission measurement has inherent limitations and restricted analytical applications. At low concentrations recording XAS spectra in the fluorescence mode is more sensitive than in the transmission mode. In fluorescence measurements efficient detection of the radiation is necessary and arrays of solid state detectors are used. Transmission and fluorescence measurements are not easily interpretable, but interpretations can be based on the relation of spectral features with those of model compounds.

The most important application in the environmental field is individual particle analysis within the framework of atmospheric chemistry studies. Particulate material produced by the biosphere, in the oceans or injected into the atmosphere by phenomena such as volcanoes, has been implicated as perturbing the delicate climatic balance between absorption of incoming solar radiation and outgoing energy. Particles affect the formation of clouds and the visibility and play a role in heterogeneous gas reactions. After having been removed from the atmosphere by rain, snow, *etc.*, they may contribute to the pollution of waters and soils and have an adverse effect on fauna and flora. Pollution produced particles have, in addition, a strong effect on the local environment of cities and industrialised areas and they are a major object for studies.

Jaklevic *et al.*[46] have reported on the speciation of Zn, Fe and Cr as a function of particle size, on size fractionated air particulate material showing, *e.g.*, that Fe is distributed between $FeNH_4(SO_4)_2$ and Fe_2O_3 while Cu is present as $CuSO_4$. Zinc was predominantly present in the 'fine' fraction as $ZnSO_4$ or $Zn(NH_4)2(SO_4)_2$ while mostly as ZnO in the 'coarse' fraction. Spectra of S were too much alike to be interpretable.

For air particulate matter a significant improvement resides in the use of microanalytical mapping. Exploratory studies on individual fly ash with dimensions of 1–2 μm were reported recently by Török and co-workers.[47,48] Micrometer sized fly ash particles are of special concern. They are distinctly heterogeneous and have an irregular shape and a large size range from several hundred to submicron aerodynamic size. This type of anthropogenic pollution aerosol is formed at high temperatures (above 1500 °C) by burning of coal or lignite in power plants and contains altered remains of the clay minerals originally present in the fuel. As a result, a highly complex material is formed onto which surface, volatile elements of high toxicity such as, *e.g.*, As can be concentrated. Since a fraction of the fly ash is inhalable, this type of material presents

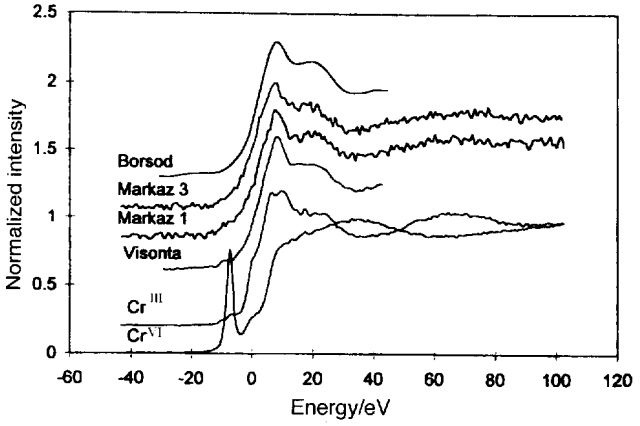

Fig. 14 XANES spectra of Cr^{3+}, Cr^{6+} and fly ash particles (Osan *et al.*, ref. 48).

a health hazard and it is appropriate to study its formation mechanism in detail.

XANES measurements on Fe showed the presence of significant amounts of hematite, as was further corroborated on the bulk samples with Mössbauer spectrometry. For Cr, the absence of a pre-edge peak characteristic for Cr^{6+} indicated that the particular lignite burning produced fly ash contained the less toxic Cr^{3+}. The experimental results demonstrate that synchrotron X-ray microscopy can be used as a tool for investigating the chemical composition of selected elements on micron-sized particles. XANES spectra for Cr^{3+} and Cr^{6+} standards and several single fly ash particles produced in a power station in Hungary (Borsod) and in Gyöngyösvisonta[48] are shown in Fig. 14.

Another recent report dealt with the measurement of Si and S in coal fly ash particles by low energy EXAFS. Recording both the sample current resulting from the electrons emitted from the sample and the fluorescence radiation as a function of the incident X-ray energy, it appeared possible to obtain surface (100–1000 nm) and bulk chemical information. In pre-fractionated fly ash chemical differences were observed such as S^{6+} in the surface region and S^{2-} in the bulk of the particles.[49]

X-ray microdiffraction and microtomography

Two other powerful tools can be used with a microscopic X-ray beam. The diffraction pattern can be measured over a complex sample and provides information on the variation of its crystallographic structure on a level commensurate with the X-ray beam.

Computerized tomography (CT) is now a well-established technique in diagnostic radiology. The main obstacle in employing the method at a high spatial resolution resides with the photon flux available. When absorption or fluorescence radiation from a SR microbeam is measured systematically, as it is impinging on a sample it is possible to reconstruct its shape, density and composition. Contrast for specific features in the object can be achieved by exploiting features of the X-ray absorption spectrum. The energy of the beam also allows the selection of a suitable penetration depth. Theoretical–methodological development is now in progress for the experimental verification of a quantitatively reliable back projection model for XRF tomography. Models are necessary to be able to convert raw experimental data into three-dimensional concentration information on the analysed materials. This area is undergoing rapid development.[50]

Phase contrast imaging

With the high spatial and time coherence of the X-ray beam delivered at third generation SR sources, it is possible to observe very weak perturbations of the wavefront, resulting in phase contrast. The effect is fairly sensitive as the decrement of the refractive index [δ in eqn. (1)] is *ca.* 1000 times more intense than the radiation absorption coefficient, but only intensity not phase of wave can be measured and the edges of the image are enhanced. Hence, it becomes possible to realise phase contrast imaging directly from a sample in the transmission geometry. Absorption (reconstruction of the absorption index in the object) and phase contrast tomography (reconstruction of the refractive index) are possible.

As was shown by Snigirev *et al.*,[51] Raven *et al.*[52] and Koch *et al.*[53] well-collimated coherent beams at 10–50 keV at the ESRF beamlines make visible very small light density objects, such as organic fibers, which do not practically absorb the incident radiation and only produce an inhomogeneous phase shift of the wavefront of the radiation. The results obtained up to now show that phase contrast microscopy, phase contrast tomography, interferometry and holography are possible at the μ-FID_{22} and other beamlines, thus supplementing the analytical possibilities with microscopic, even submicroscopic observational tools. The elements of the optical set-up of the μ-FID_{22} such as beryllium windows, filters and windows of the beamline are specially polished to allow effective use of this tool.[54]

APPLICATIONS

In what follows two applications of μ-XRF using first a second generation SR for archaeological analysis and then the ESRF third generation synchrotron source for the analysis of environmental particulate matter will be described.

Determination of rare earth elements in fossilised bones

The X-ray microfluorescence spectrometer at the Hamburg Hasylab laboratory described earlier has been used for the determination of the distribution of trace concentrations of rare earth elements (REEs) in two 1.2–1.8 million year old fossilized bones from different depositional environments in Olduvai (Tanzania).[55] The data could help to provide information on the dietary and nutritional habits of these early populations. The SR source was selected for this work because the excitation spectrum reaches into the very hard X-ray region (70–100 keV) and allows the determination of the high atomic number elements by means of their K-radiation.

Janssens *et al.*[56] described results of quantitative determinations at the minor and trace level (ppm) which indicate that the microdistribution of the REEs is not homogeneous and that the relative abundance of these elements can provide information on the paleo-environmental information during the fossilization process. The results were also critically compared with those obtained by other methods, such as instrumental neutron activation analysis[57] and laser ablation inductively coupled plasma mass spectrometry.[57] The advantage of the SR-XRF is that is is possible to obtain the lateral distribution of the REEs and other elements with a spatial resolution of *ca.* 20 μm. A limitation is that with short spectrum collection times, the detection limits are only in the range of 5–10 ppm, making it impossible to apply to weakly enriched elements. Such measurements could gain enormously in importance (spatial resolution and detection limits) when more brilliant SR sources are applied. A typical profile through a bone for Y, La, Ce and Pr is given in Fig. 15.[57]

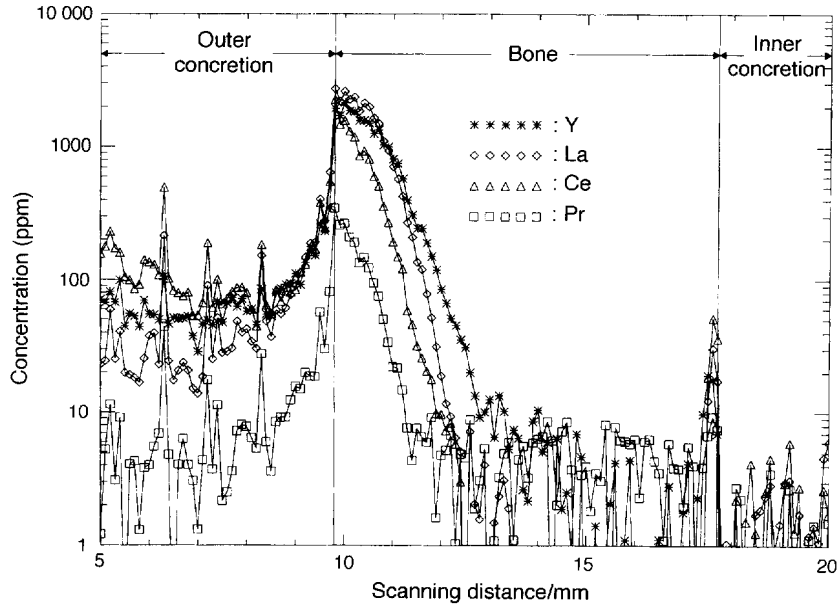

Fig. 15 Concentration profiles of Y, La Ce and Pr obtained for sample OLD-8.10. Step size; 100 μm; and collection time per step; 100 (ref. 59).

Characterization of air particulate matter

The use of sensitive XRF microanalysis on particle aggregates, on size fractionated samples and on individual particles provides multi-element concentrations at the ppm, even the sub-ppm level as has been demonstrated in a number of exploratory studies as mentioned above. At current SR-XRF facilities, only particles with a diameter above *ca.* 10 μm can be readily analysed; in this size range, however, the sensitivity of SR-XRF for heavy elements was shown to be superior to that of μ-PIXE.[58] At the ESRF facility, analysis of smaller particles (with diameter down to about 1 μm) will be possible and in a significantly shorter analysis time.[60]

To illustrate the new analytical capabilities for particle characterization created by third generation sources such as ESRF, the microscopic composition and crystallographic structure of fly ash collected from a lignite-fired power station in Japan by a combination of XRF and XRD was studied at BL1 of ESRF during pilot experiments, recently described by Rindby *et al.*[61] in a scanning mode with a 1–2 μm lateral resolution. Two-dimensional images of different analytical information were reconstructed from the data recorded during the scans, taking into account parameters such as depth distribution and sample surface topgraphy, which disturb direct quantification of the XRF response. For XRF the microbeam set-up is capable of determining trace elements down to the sub-ppm level with a minimum detectable amount of less than 10^{-16} g, demonstrating that the technique allows real trace element capability on the scale of 2 μm. For XRD, the data recorded from each pixel is a diffraction pattern. For a complex material such as fly ash, each individual pattern consists of a number of individual reflection points superimposed on a number of diffraction rings. The image of well defined single reflections that can be attributed to a particular crystallographic system or mineral (*e.g.*, quartz or mullite) can be reconstructed from the dataset, allowing the mapping of type, orientation and size of different monocrystalline, polycrystalline and amorphous phases.

It became evident from this preliminary study that the combination of XRF and XRD imaging gives new information on the thermodynamic conditions during the formation and the early history of particles. In addition, other types of analytical methods such as small angle scattering (SAXS) or XANES might also be applicable simultaneously with XRD and XRF and thus would provide more information on the microchemistry of the objects.

Thanks are due to the FWO, Brussels, Belgium for the support of this work.

REFERENCES

1 *Handbook of X-Ray Spectrometry*, ed. Van Grieken, R., and Markowicz, A. A., Marcel Dekker, New York, 1993.
2 *Quantitative X-ray Spectrometry*, ed. Jenkins, R., Gould, R. W., and Gedcke, D., 2nd edition, Marcel Dekker, New York, 1995.
3 Lachance, G. R., and Claisse, F., *Quantitative X-ray Fluorescence Analysis: Theory and Application*, John Wiley, New York, 1995.
4 Johansson, S. A. E., Campbell, J. L., and Malmqvist, K. G., *Particle Induced X-ray Emission Spectrometry, (PIXE)*, John Wiley, New York, 1995.
5 Malmqvist, K., *X-ray Spectrom.*, 1995, **24**, 226.
6 Vekemans, B., Janssens, K., Vincze, L., Adams, F., and Van Espen, P., *Spectrochim. Acta, Part B*, 1995, **50**, 149.
7 Schneider, B., *Spectrochim. Acta, Part B*, 1989, **44**, 519.
8 Injuk, J., and Van Grieken, R., *Spectrochim. Acta, Part B*, 1995, **50**, 1787.
9 Williams, G., *Synchrotron Radiat. News*, 1997, **10**, 2.
10 Vincze, L., Janssens, K., Adams, F., Rivers, M. L., and Jones, K. W., *Spectrochim. Acta, Part B*, 1995, **50**, 127.
11 Vincze, L., Janssens, K., Adams, F., and Jones, K. W., *Spectrochim. Acta, Part B*, 1995, **50**, 1481.
12 Rindby, A., Voglis, P., and Attaelmanan, A., *X-ray Spectrom.*, 1996, **25**, 39.
13 Tougaard, S., *Surf. Interface Anal.*, 1997, **25**, 137.
14 Wherry, D., and Cross, B. J., *Spectrosc. Int.*, 1988, **1**, 57.
15 Wherry, D. C., Cross, B. J., and Briggs, T. H., *Adv. X-ray Anal.*, 1988, **31**, 93
16 Vincze, L., Ph.D. Thesis, University of Antwerpen, 1995.
17 Haensel, R., *Nucl. Instrum. Methods, Sect. A*, 1988, **266**, 68.
18 Glanz, J., *Science*, 1995, **267**, 1904.
19 Iida, A., *Trends Anal. Chem.*, 1991, **10**, 215.
20 Smith, J. V., *Conf. Ser. Inst. Phys.*, 1992, **160**, 605.
21 Vincze, L., Janssens, K., and Adams, F. C., *Conf. Ser. Inst. Phys.*, 1992, **160**, 605.
22 Chapman, K. L., Thomson, A. L., and Underwood, J. H., *Proceedings of the 42nd Denver Conference on Applications of X-ray Analysis*, Denver Co, USA, August 2–6, 1993, book of abstracts, p. 119.
23 Snigirev, A., Kohn, V., Snigireva, I., and Lengerer, B., *Nature (London)*, 1996, **384**, 49.
24 Elleaume, P., *ESRF Newsl.*, 1997, **28**, 33.

25 Bilderback, D. H., Thiel, D. J., Pahl, R., and Brister, K. E., *J. Synchrotron Rad.*, 1994, **1**, 37.
26 Dabagov, S. B., Kurnakhov, M. A., Nikitina, S. V., Murashova, V. A., Fedorchuk, V., and Yakimenko, M. N., *J. Synchrotron Rad.*, 1995, **2**, 132.
27 Engström, P., Rindby, A., and Vincze, L., *ESRF Newsl.*, 1996, **26**, 30.
28 *X-ray Science and Technology*, eds. Michette, A. G., and Buckley, C. J. IOP Publishing, Bristol, 1993.
29 Singirev, A., *Rev. Sci. Instrum.*, 1995, **66**, 2053.
30 Pella, P. A., Feng, L., *Adv. X-ray Anal.*, 1992, **35**, 1063.
31 Boehme, D. R., *Adv. X-ray Anal.*, 1987, **30**, 39.
32 Rindby, A., Engström, P., Larsson, S., and Stocklassa, B., *X-ray Spectrom.*, 1989, **18**, 109.
33 Larsson, S., Engström, P., and Rindby, A., *Adv. X-ray Anal.*, 1990, **33**, 623.
34 Shakir, N., Larsson, S., Engström, P., and Rindby, A., *Nucl. Instrum. Methods, Sect. B*, 1990, **52**, 194.
35 Janssens, K., Vekemans, B., Vincze, L., Adams, F., and Rindby, A., *Spectrochim. Acta, Part B*, 1996, **51**, 1661.
36 Vekemans, B., Janssens, K., Vincze, L., Adams, F., and Rindby, A., *X-ray Spectrom.*, 1994, **23**, 278.
37 Vincze, L., Janssens, K., and Adams, F., *Adv. X-ray Anal.*, 1994, **37**, 553.
38 Jones, K., and Gordon, B. M., *Anal. Chem.*, 1989, **61**, 341A.
39 Vladimirsky, Y., Kern, D. P., Chang, T. H. P., Attwood, D. T., Iskander, N., Rothman, S., McQuaide, K., Kirz, J., Ade, H., McNulty, I., Rarback, H., and Shu, D., *Nucl. Instrum. Methods, Sect. A*, 1988, **266**, 324.
40 Anon., *ESRF Beamline Handbook*, www.esrf.fr/exp-facilities/BLHB.htm.
41 Janssens, K., Vincze, L., and Adams, F., *Anal. Chim. Acta*, 1993, **283**, 98.
42 Görgl, R., Wobrauschek, P., Kregsamer, P., Streli, Ch., Haller, M., Knöchel, A., Radtke, M., *X-ray Spectrom.*, 1997, **26**, 189.
43 Anon., *Spectrochim. Acta, Part B*, 1991, **46**, special issue.
44 Schwenke, H., Knoth, J. in *Handbook on X-ray Spectrometry*, eds. Van Grieken, R. E., Markowics, A. A., Marcel Dekker, New York, 1993, p. 453.
45 Ade, H., Zhang, X., Cameron, S., Costello, C., Kirz, J., and Williams, S., *Science*, 1992, **258**, 972.
46 Jaklevic, J. M. Kirby, J. A., Ramponi, A. J., and Thomson, A. C., *Environ. Sci. Technol.*, 1980, **14**, 437.
47 Török, S., Faigel, G., Jones, K. W., Sutton, S. R., and Bajt, S., *X-ray Spectrom.*, 1994, **23**, 3.
48 Osan, J., Török, B., Török, S., Jones, K. W., *X-ray Spectrom.*, 1997, **26**, 37.
49 Kawai, S., Hayakawa, F., Esaka, F., Zheng, S., Kitajima, Y., Maeda, K., Adachi, H., Goshi, Y., and Furuya, K., *Anal. Chem.*, 1995, **67**, 1526.
50 Haddad, W. S., McNulty, I., Trebes, J. E., Anderson, E. H., Levesque, R. A., and Yang, L., *Science*, 1994, **266**, 1213.
51 Snigirev, A., Snigireva, I., Kohn, V., Kuznetsov, S. M., and Scelokov, I., *Rev. Sci. Instrum.*, 1995, **66**, 5486.
52 Raven, C., Snigirev, A., Snigireva, I., Spanne, P., Souvorov, A., and Kohn, J., *Appl. Phys. Lett.*, 1996, **69**, 1826.
53 Koch, A., Raven, C., Spanne, P., and Snigirev, A., *J. Opt. Soc. Am. (B)*, submitted for publication.
54 Snigirev, A., Snigireva, I., Kohn, V., and Kuznetsov, S. M., *Nucl. Instrum. Methods, Sect. A*, 1996, **370**, 634.
55 Patterson, C. C., Shirahata, H., and Ericson, J. E., *Sci. Total Environ.*, 1987, **61**, 167.
56 Janssens, K., Vincze, L., Vekemans, B., Williams, C. T., Radtke, M;, Haller, M., and Knöchel, A., *Fresenius' J. Anal. Chem.*, 1997, in the press.
57 Williams, C. T., in *Trace Elements in Environmental History*, ed. Grupe, G., and Hermann, B., Springer Verlag, Berlin, 1988.
58 Chenery, S., Williams, C. T., Elliot, T. A., Forey, P. L., and Werdelin, L., *Microchim. Acta*, 1996, **13**, 259.
59 Janssens, K., Vekemans, B., Adams, F., Van Espen, P., and Mutsaers, P., *Nucl. Instrum. Methods, Sect. B*, 1996, **109/110**, 179.
60 Engström, P., and Riekel, C., *J. Synchrotron Rad.*, 1996, **3**, 97.
61 Rindby, A., Engström, P., and Janssens, K., *J. Synchrotron Rad.*, 1997, **4**, 228.

Paper 7/07100K
Received October 1, 1997
Accepted December 2, 1997